Sulfur-induced embrittlement of nickel: a first-principles study

2012 Modelling Simul. Mater. Sci. Eng. 20 065007

(http://iopscience.iop.org/0965-0393/20/6/065007)

Modelling Simul. Mater. Sci. Eng. **20** (2012) 065007 (15pp) doi:10.1088/0965-0393/20/6/065007

Sulfur-induced embrittlement of nickel: a first-principles study

Georg Schusteritsch and Efthimios Kaxiras

Department of Physics and School of Engineering and Applied Sciences, Harvard University, Cambridge, MA 02138, USA

E-mail: schust@fas.harvard.edu

Received 5 April 2012, in final form 23 June 2012
Published 23 July 2012
Online at stacks.iop.org/MSMSE/20/065007

Abstract

We study the embrittlement of Ni due to the presence of S impurities, considering their effect in the bulk and at grain boundaries (GBs). For bulk Ni, we employ Rice's theory based on generalized-stacking-fault energetics and the unstable stacking energy criterion. We use first-principles density-functional-theory calculations to determine the ductility parameter $D = \gamma_s/\gamma_{us}$, the ratio of the surface energy γ_s to the unstable stacking energy γ_{us}, for bulk Ni with substitutional S impurities. Similar arguments based on Rice's theory for the mechanical properties of GBs are invoked. We study the $\Sigma 5(0\,1\,2)$ GB with interstitial S impurities, in which case D is defined as the ratio of the work of separation W_s and the unstable stacking energy γ_{us}, to model the competition between grain decohesion and shear-induced plastic deformation due to grain boundary sliding (GBS). The presence of S impurities is found to increase the value of D by $\sim$40% in bulk Ni, but reduces it by over 80% for the GB. These results support earlier suggestions that embrittlement of Ni by S impurities is related to their effect on GBs. We further calculate relevant tensile and shear stresses to study the expected fracture mode and find that intergranular crack propagation accommodated by GBS is inhibited in the system considered here.

(Some figures may appear in colour only in the online journal)

1. Introduction

Embrittlement of ductile metals by chemical impurities is a process of great importance in materials used in a wide range of technologies, ranging from transportation to the energy industry. Although this process has been known in the industry for a long time, the fundamental mechanisms underlying chemical embrittlement are not understood at the atomic level. More detailed knowledge of atomistic level processes can lead to improvements in the design and efficiency of many practical applications. In this study we concentrate on the effects of

S impurities on the mechanical properties of Ni. This system is of great industrial interest since nickel-based alloys are widely used, whilst sulfur is a common impurity during processing steps and in many operating environments.

Much experimental effort has been devoted to the study of S impurities in Ni. These impurities segregate at the grain boundaries (GBs) [1–9] and lead to a transition from ductile transgranular to brittle intergranular fracture at high concentrations in microcrystalline materials [1–7]. Recent experimental work identified a critical S impurity concentration for this transition, accompanied by amorphization [9]. Theoretical work addressed some of these issues of chemical embrittlement from an atomistic viewpoint. Chen *et al* [10] performed large-scale molecular dynamics (MD) simulations supporting the experimental work by Heuer *et al* [9]. Yamaguchi *et al* [11] used first-principles density-functional-theory calculations to provide theoretical evidence for the segregation effect of sulfur near GBs and showed how this effect leads to weakening of the structure by decohesion. Kart *et al* [12] were able to confirm those results. Similarly, Sanyal *et al* [13] studied the effects of different impurities on the decohesion of a Ni GB and related this to chemical embrittlement.

Most of these experimental and theoretical studies have addressed the behavior and processes in coarse-grained materials. Recent advances in processing techniques have enabled selective growth of ultrafine crystalline (ufc) and nanocrystalline (nc) materials. GB engineering techniques have enabled control over the GB structure. Manipulating the grain sizes and the GB structure may result in enhancements in the mechanical properties. Kobayashi *et al* [6], for instance, have shown that special GBs have higher resistance to S embrittlement in ufc Ni. At the same time, these techniques make a deeper understanding of the underlying atomic-scale processes more important in order to effectively take advantage of the microstructure. For example, different response mechanisms are thought to apply to coarse-grained than nc metals. Several classical MD studies have highlighted the importance of intergranular deformation mechanisms in nc metals [14–19]. These results were instrumental in showing that in contrast to coarse-grained metals, GBs in nc metals do not merely act as static barriers for crystal dislocations. Instead, as grain sizes become smaller, the GBs themselves play an increasingly important role in plastic deformation and fracture [14–19]. In this context plastic deformation can be facilitated by GB sliding (GBS). Most theoretical and computational studies to date, that addressed chemical embrittlement of Ni from an atomistic level, have considered the decohesion behavior of GBs [11–13] but not shear effects, which could be of crucial importance.

The mechanical behavior of solids is inherently connected to the issue of brittle or ductile response. The terms ‘brittle’ and ‘ductile’ refer to macroscopic response, which ultimately is related to the atomic-scale structure and nature of bonding between atoms in the solid. The connection between macroscopic behavior and atomic-scale structure is not trivial, and remains the focus of vigorous research in many classes of materials. Armstrong [20] and Kelly *et al* [21] first suggested that the difference between the two types of responses is due to competition between decohesion (also referred to as ‘Griffith cleavage’) and plastic deformation (or shear) at the tip of a crack inside the solid; these ideas were subsequently put on a more quantitative basis first by Rice and Thomson [22] and later by Rice [23] who related the decohesion and shear tendencies to specific energy terms that can be ultimately connected to the atomic structure of the solid. This provided a criterion for determining the brittle or ductile response of the solid by calculating the relevant energy terms, from atomic-scale considerations. The approach based on Rice’s criterion [23] for brittle versus ductile behavior can give a clear picture of the effect of the chemical composition of the solid and of changes in it, for example, the introduction of impurities on the mechanical properties. We extend the original Rice’s theory to study ductile versus brittle response at GBs of small-sized grains, by considering the competition between

plastic deformation facilitated by shear in the form of GBS and brittle response induced by grain decohesion. Specifically, we examine whether or not S impurities at GBs in Ni are the dominant mechanism for its embrittlement. To this end, we calculate the decohesion energy and unstable stacking energies both for bulk Ni and for a representative GB in Ni, and compare these values for the pure structures and structures with S impurities at the relevant slip and decohesion planes. Our results show that in bulk Ni, the presence of S impurities leads to an *increase* in ductility. In contrast to this, we find clear evidence of S-induced embrittlement for the case of the Ni GB, introduced by a decrease in the required work of separation and suppression of GBS. This supports the view that S impurity segregation at the Ni GBs is a dominant effect in its embrittlement.

The paper is organized as follows: in section 2 we present the theoretical framework for interpreting our first-principles calculations in the context of macroscopic continuum theory, together with a description of our specific computational model. Section 3 presents the results of our calculations for the key quantities that characterize brittle or ductile response for bulk Ni and the Ni GB, with or without the S impurities. Finally, in section 4 we discuss our conclusions.

2. Theoretical framework

Macroscopic theories have been used extensively to describe the mechanical behavior of materials. Early work by Rice and Thomson [22] modeled the process of nucleation of dislocations at the tip of a crack as the fundamental mechanism of plastic shear. Subsequently, Rice [23] used the Peierls concept [24] to quantify the competition between cleavage and plastic shear at the tip of a crack, which are related to brittle versus ductile response of a stressed solid, in terms of two key quantities: the surface energy of newly exposed surfaces due to cleavage, γ_s, and the unstable stacking energy, γ_{us}, the lowest energy barrier for sliding two halves of a periodic crystal over a full period across a crystal plane. Using this theoretical framework, studies of representative solids with effective interatomic potentials [25] or first-principles total-energy calculations [26] were carried out to elucidate the nature of brittle or ductile response of various materials. Extensions of these studies to more realistic situations [27–29] were employed to predict the change in mechanical response due to impurities [30, 31]. Thus, the combination of Rice's continuum macroscopic theory, coupled with high-accuracy atomistic scale calculations for the values of key quantities such as γ_s and γ_{us}, can be useful for addressing qualitatively the complicated issue of brittle versus ductile behavior in the presence of chemical impurities.

In this approach, the main point is that a large value of the ratio $D = \gamma_s/\gamma_{us}$, called the ductility parameter [32], implies ductile behavior because it corresponds either to a large energy cost for cleavage (large γ_s) or to a small energy cost for dislocation nucleation (small γ_{us}); conversely, a small value of D implies brittle behavior due to a small cost of cleavage (small γ_s) or large cost for dislocation nucleation (large γ_{us}). There is, however, no general rule for what constitutes 'large' or 'small' values of D in such comparisons; it depends on the specific system under consideration. For example, in what concerns the behavior of fcc metals, Rice [23] previously estimated the critical value of D to lie between 4 and 9 and was able to successfully correlate the values of the ductility parameter D of several metals with the correct experimental behavior. When the interest is specifically focused on the role of chemical impurities, the task is simpler: the values of γ_s and γ_{us} can be calculated with or without impurities, and the resulting comparison can give strong indications about the likely role of the impurities [30, 31]. The use of first-principles quantum mechanical calculations that faithfully represent the chemical character of various species of atoms makes it possible to obtain accurate values for γ_s and γ_{us},

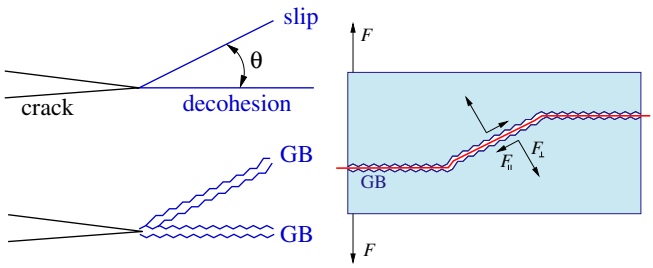

Figure 1. Illustration of slip/decohesion planes at a relative angle θ, in the bulk (left panel, straight lines represent bulk planes), in the presence of GBs (represented by jagged lines), and possible intergranular failure mechanism (right panel, fracture along red boundary between GBs) due to external load, with forces denoted as F and their parallel $F_{||}$ and perpendicular $F_{\perp}$ components on a given GB.

at least in cases where the relevant geometries are simple enough to make such calculations feasible.

For the most part in this study we consider the simple ratio of the unstable stacking energy, γ_{us}, and the surface energy, γ_{s}, to calculate the ductility parameter D. This is sufficient when the geometries, and in particular the Burgers vectors, of the system of interest do not change significantly when impurities are present or not. When the Burgers vectors change as impurities are introduced, a more careful definition of the ductility parameter $\tilde{D}$ is required. Rice showed that, for mode I loading, the energy release rate for dislocation nucleation is [22],

$$G_{\mathrm{d}} = 8\frac{1+(1-\nu)\tan^2\phi}{(1+\cos\theta)\sin^2\theta}\gamma_{\mathrm{us}}, \tag{1}$$

where θ is the angle between the slip and decohesion planes (see figure 1) and ν is the Poisson ratio; the angle ϕ is the one subtended between the normal to the intersection of the slip and decohesion planes which lies on the slip plane and the Burgers vector [23]. The energy release rate for Griffith cleavage is $G_{\mathrm{c}} = 2\gamma_{\mathrm{s}}$. The most general definition for the ductility parameter $\tilde{D}$ is then $\tilde{D} = G_{\mathrm{c}}/G_{\mathrm{d}}$. For situations where θ and ϕ are constant $\tilde{D} = \alpha D = \alpha(\gamma_{\mathrm{s}}/\gamma_{\mathrm{us}})$, with α being a constant factor determined by geometric considerations.

We extend here the concept of the generalized energy surface, or γ-surface, first discussed by Vitek [33], to the case of a GB. Specifically, we use the work of separation (W_{s}) and the minimal energy required to shear the GB (γ_{us}), in the same spirit as these are used in relation to decohesion and slip planes in the bulk of a regular crystal. We note that the decohesion (cleavage) and slip planes in a crystal are often different [31]. In the case of a GB it is a reasonable choice to identify both the decohesion and slip planes with the GB plane, since this is the weak plane of the system on which either decohesion or slip may occur. In the context of GBs γ_{us} now quantifies the resistance against shear and can therefore still be taken as a measure of ductility. The competing process of greatest importance is that of cleavage, quantified by the work of separation (W_{s}) for intergranular decohesion along the GB. We can then define in a similar manner as in the original Rice's theory a ductility parameter as the ratio of these two competing processes $D^{\mathrm{GB}} = W_{\mathrm{s}}/\gamma_{\mathrm{us}}$. We will use the natural cleavage plane of bulk fcc Ni, the (1 1 1) plane, and the $\Sigma5(0\,1\,2)$ GB as a prototypical planar defect that has been the subject of detailed studies recently [11–13].

The total energy of various structures, from which the key quantities discussed above can be directly obtained, are calculated using density-functional-theory as implemented in the VASP code [34]. The generalized gradient approximation (GGA) [35] with projector-augmented

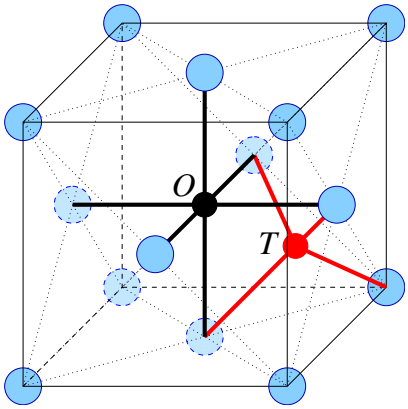

Figure 2. Illustration of the two interstitial sites in the fcc lattice: the regular lattice sites are shown as blue circles, the tetrahedral interstitial (T) is shown as a red circle and linked by red lines to its four nearest neighbors and the octahedral interstitial (O) is shown as a black circle and linked by black lines to its six nearest neighbors.

plane wave (PAW) potentials [36] was used for all calculations. We elected to perform spin polarized calculations to improve accuracy, since Ni can be a magnetic solid. A kinetic energy cutoff of 330 eV was used after carefully testing for convergence when the geometry of the system is changed during slip calculations and when S impurities were included. The Methfessel–Paxton smearing of second order [37] was used with a smearing width of 0.1 eV. All relaxations were performed using the conjugate-gradient method as implemented in VASP. Finally, a uniform Monkhorst–Pack [38] k-point grid of $15 \times 15 \times 15$ was used for the fcc bulk Ni calculations with four atoms in the cubic unit cell and scaled appropriately for larger supercells (for instance, a $2 \times 2 \times 1$ grid was used for the supercell with a GB, as in similar works [11, 12]).

With these computational parameters, we determined the lattice constant for fcc Ni by fitting the Birch–Murnaghan equation of state, which results in a lattice constant of $a = 3.52$ Å and a bulk modulus of $B = 185.8$ GPa which compare well with the experimentally determined values of $a = 3.52$ Å [39] and $B = 186$ GPa [39]. Relaxation of the unit cell volume was explicitly taken into account when impurities are introduced in the host crystal.

3. Results and discussion

We address first the question of where the S impurities sit in the case of the fcc bulk structure and the $\Sigma 5(0\,1\,2)$ GB. For bulk Ni, in general, impurities can be accommodated at either interstitial or substitutional sites. There are two interstitial positions in the fcc lattice where impurities typically reside [40], the so-called 'tetrahedral' (T) and 'octahedral' (O) sites, named after the coordination of these sites with nearest neighbor regular lattice sites; the position of these defects in the lattice is indicated in figure 2.

To determine the optimal position for the impurities we calculated the formation energy $\varepsilon_{\mathrm{f}}^{X}$ per impurity, defined as

$$\varepsilon_{\mathrm{f}}^{X} = \frac{1}{n_{\mathrm{i}}}\left[E_{\mathrm{tot}}^{X}(n_{\mathrm{i}}, n_{\mathrm{h}}) - E_{\mathrm{tot}}\left(n_{\mathrm{h}}^{0}\right) - n_{\mathrm{i}}\mu_{\mathrm{i}} - \left(n_{\mathrm{h}} - n_{\mathrm{h}}^{0}\right)\varepsilon_{\mathrm{h}}\right] \tag{2}$$

where $E_{\mathrm{tot}}^{X}(n_{\mathrm{i}}, n_{\mathrm{h}})$ is the total binding energy of the system containing n_{i} impurities of type X ($X = I_{\mathrm{T}}$ or I_{O} for the interstitial tetrahedral and octahedral positions in bulk Ni, and S for the

Table 1. Formation energies ε_f^X (in eV) from equation (2) of the various S point defects in bulk Ni and at the $\Sigma5(0\,1\,2)$ GB, for the S chemical potential $\mu_S = -3.22$ eV (corresponding to bulk S, consisting of stacked octagonal rings). $X = I_T$, I_O are the bulk interstitial positions (tetrahedral and octahedral, respectively), $X = S_b$ is the bulk substitutional position, I_{GB}, S_{GB} are the GB interstitial and substitutional positions. Bulk concentrations Θ correspond to percentage of impurities in the supercell; GB concentrations correspond to the defect plane ratio for the GB0 plane.

X	Θ	ε_f^X
I_T	0.92%	3.16
I_O	0.92%	1.96
S_b	0.93%	0.38
I_{GB}	0.25	−0.89
I_{GB}	1.0	−1.21
S_{GB}	0.33	0.35

substitutional positions), and n_h atoms of the host crystal, $E_{tot}(n_h^0)$ is the total binding energy of the system without impurities containing n_h^0 host atoms, μ_i is the chemical potential for the impurities and ε_h is the binding energy per atom of the host crystal in its ideal structure. In this expression, the supercell is chosen so that $n_i \ll n_h$ (ideally, $n_h \to \infty$). We have considered two different reservoirs for S, isolated S atoms (equivalent to the limit of $\mu_S = 0$) and bulk S, which consists of puckered hexagonal or octagonal stacked rings of S [41]. To obtain the bulk S chemical potential, we optimized the structures using the same computational parameter as for bulk Ni and a cubic supercell of large size (with lattice constant up to 28 Å), and found that in the hexagonal rings the S–S bond length is 2.06 Å and the S–S–S bond angle is 102°, whereas for the octagonal rings the bond length is 2.04 Å and the bond angle is 108°. The difference in chemical potential between the hexagonal and octagonal rings is only 0.07 eV in favor of the latter, so we will quote results in the rest of the paper for the octagonal ring structure only, which corresponds to $\mu_S = -3.22$ eV. The results of these calculations for the formation energy of S point defects in bulk Ni are given in table 1. We find that the energies of formation of the S interstitial defect at both the tetrahedral and octahedral positions are $I_T = 3.16$ eV and $I_O = 1.96$ eV, respectively. This is significantly greater than the formation energy of a substitutional S defect, namely $S_b = 0.38$ eV. These results suggest that the only relevant S defect in bulk Ni is the substitutional.

We have performed similar calculations for the formation energy of impurities at the GB plane. The open spaces on the GB plane allow energetically favorable interstitial S impurities (this is explained in more detail in section 3.2). In the context of the following calculations of the unstable stacking and decohesion energies, it is useful to introduce at this point a convenient measure of the impurity concentration on a defect plane. We follow the literature convention [42] of defining the defect plane impurity concentration Θ as the ratio of the number of S atoms to the number of Ni atoms on the respective defect plane. The planes used throughout will be the cleavage or slip planes. Table 1 summarizes the formation energies for the case of one and four S atoms in a unit cell containing four Ni atoms on each plane parallel to the GB plane, that is, for $\Theta = 0.25$ and 1.0 (see figure 5). These values include supercell volume relaxation. The unit cell volume for the GB with impurities increases: the lattice constant perpendicular to the GB plane ($a_3 = 16.40$ Å in the pure Ni case) expands by 1% and 3% for $\Theta = 0.25$ and 1.0, respectively; of the other two lattice vectors in the plane parallel to the GB, one ($a_1 = 7.02$ Å in the pure Ni case) contracts by 1% for both S concentrations, and the other ($a_2 = 7.85$ Å in the pure Ni case) expands by 1% and by 2% for $\Theta = 0.25$ and 1.0, respectively. The energy gain due to the volume relaxation is very small and the S inclusion energy dominates. The formation energies in this case are considerably lower than for bulk Ni. This finding indicates

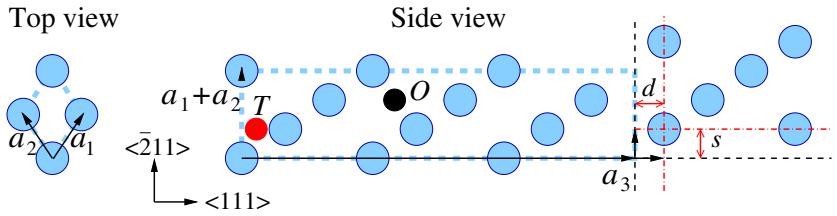

Figure 3. Setup for the calculation of γ_s and γ_{us} in bulk fcc Ni: Ni atoms are represented by blue circles. The top view shows the unit cell vectors $\boldsymbol{a}_1, \boldsymbol{a}_2$ on the (1 1 1) plane. The side view shows the atoms along the $\langle 1\,1\,1\rangle$ crystal direction, with the corresponding lattice constant a_3. The thick dashed blue line represents the boundary of the supercell in the ideal crystal, which contains 9 (1 1 1) planes of atoms. Changes in the supercell lattice constant (indicated by the small vertical and horizontal arrows) define the distortions through which γ_s and γ_{us} are determined: these distortions are shown as double-headed arrows d (for decohesion) and s (for slip), and correspond to a displacement of atomic planes from their positions in the ideal crystal, indicated by black dashed lines, to new positions, indicated by dashed–dotted red lines. The red circle labeled T and the black circle labeled O indicate the tetrahedral and octahedral interstitial sites in the bulk.

that S atoms segregate at the GBs under thermodynamic equilibrium conditions, but it does not address the kinetic issue, that is, how easily S atoms diffuse to the optimal equilibrium sites at the GB. A detailed study explicitly treating S diffusion from first principles is beyond the scope of this work. Experimentally it is known that S diffuses to the GB [1–9], which is consistent with our results of low-energy positions of S impurities being associated with the GB. The concentrations were chosen with experiments in mind [3, 9]: for $\Theta = 1.0$ in our case, the equivalent concentration to experimental ones would be approximately 9%, taking into account the total amount of Ni atoms that the supercell contains in the neighborhood of the GB.

3.1. Decohesion in bulk fcc Ni

We begin with a description of the unit cell for calculating the surface energy, γ_s, and unstable stacking energy, γ_{us}, for bulk Ni. The relevant plane for such calculations, on which both decohesion (cleavage) and slip take place in the fcc crystal is the (1 1 1) plane; this is illustrated in figure 3. The surface energy is determined by increasing the length of the supercell vector $\boldsymbol{a}_3$ along the $\langle 1\,1\,1\rangle$ crystallographic direction by d until the energy reaches an asymptotic value which is $2\gamma_s$ higher than the equilibrium energy. For consistency, we use the universal binding energy relation (UBER) [43] to fit the results of changing the value of d, in order to determine the asymptotic value for $d \to \infty$.

To find the surface energy, γ_s, for bulk fcc Ni decohesion in the $\langle 1\,1\,1\rangle$ direction, we also need to specify how the atoms relax in the process of separating the two halves of the crystal while exposing two (1 1 1) planes. For an unambiguous definition of the decohesion distance d, the atoms on either side of the cut must be at a fixed distance in the $\langle 1\,1\,1\rangle$ direction. Since for the calculations of the bulk decohesion the periodicity on the (1 1 1) plane is that of the bulk structure, the above restriction implies that all atoms on the two planes immediately adjacent to the cut are fixed in all directions, at the required distance d between the planes. All other atoms in the unit cell are allowed to relax fully.

For the decohesion calculation in the presence of S impurities, we used a supercell with 2×2 periodicity in the $\boldsymbol{a}_1$ and $\boldsymbol{a}_2$ lateral directions. This allows us to consider different concentrations of S impurities, by replacing one or more of the Ni atoms on the plane next to the cut by S atoms. We have considered two cases for the cleavage plane, $\Theta = 0.33$ (one

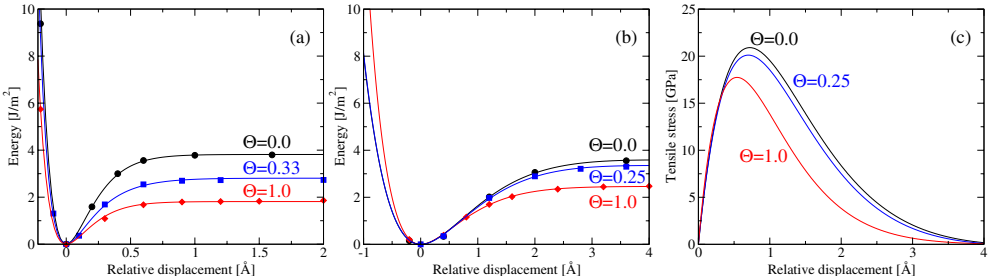

Figure 4. (*a*) Decohesion energy for bulk (1 1 1) Ni, without impurities ($\Theta = 0.0$) and at two S impurity concentrations, $\Theta = 0.33, 1.0$ (see text for details). (*b*) Decohesion energy for the $\Sigma5(0\,1\,2)$ GB without impurities ($\Theta = 0.0$) and at two S impurity concentrations, $\Theta = 0.25, 1.0$ (see text for details). (*c*) Corresponding tensile stress for the GB, without and with S impurities.

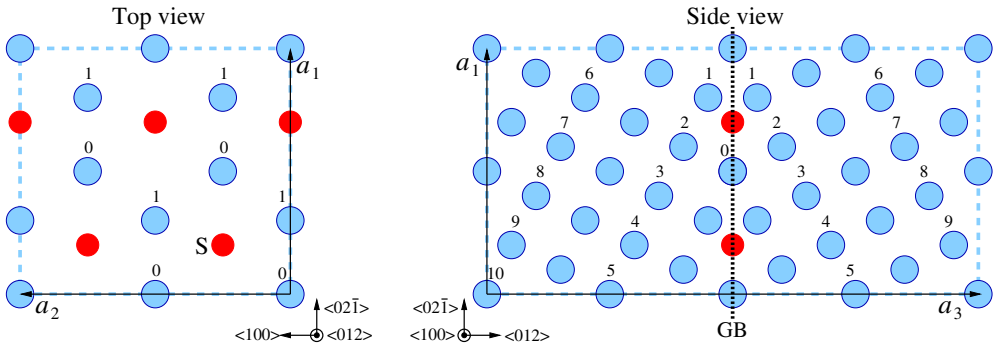

Figure 5. Setup for the calculation of the $\Sigma5(0\,1\,2)$ GB: Ni atoms are represented by blue circles, possible interstitial positions for S atoms are indicated by smaller red circles. The top view shows the unit cell vectors $\boldsymbol{a}_1, \boldsymbol{a}_2$ on the $(0\,1\,2)$ plane, parallel to the GB. The side view shows the atoms along the $\langle 0\,1\,2\rangle$ crystal direction, with the corresponding lattice constant a_3. The thick dashed blue line represents the boundary of the supercell, which contains 20 $(0\,1\,2)$ planes of atoms, labeled $-9, \ldots, 0, \ldots, 10$ (only one atom per plane is labeled). Each plane contains 4 atoms, labeled in the top view for planes 0 and 1. There are two GBs in each unit cell, at planes labeled 0 and 10. Decohesion calculations are performed by increasing the magnitude of $\boldsymbol{a}_3$ by d and moving all atoms in the top half of the cell by the same amount so that a gap appears at GB0. GSF energy calculations are performed by displacing all the atoms in one half of the crystal (defined by a cut between GB0 and GB1) with respect to the other.

substitutional S atom in the 2×2 supercell) and $\Theta = 1.0$ (two substitutional S atoms in the 2×2 supercell). These concentrations were chosen primarily in order to be able to have a direct comparison with the concentrations in the case of the GB calculations. The results of the decohesion calculations are shown in figure 4(*a*). The surface energy decreases by 27% in the case of $\Theta = 0.33$ on the cleavage plane and by 51% in the case of $\Theta = 1.0$.

3.2. Decohesion in fcc Ni with a GB

For the GB calculations we consider a $\Sigma5(0\,1\,2)$ structure, the same as in recent other work [11–13]. This GB has energetically and structurally advantageous interstitial sites for the incorporation of S impurities. The structure of this GB is shown in figure 5. The S impurities in our calculations of the work of separation are added to the four interstitial sites on the GB0 plane, equidistant from the three adjacent Ni atoms as shown in figure 5. The inclusion

Table 2. Surface (γ_s) and unstable stacking (γ_{us}) energies and ductility parameter (D) for the bulk Ni; work of separation (W_s) and unstable stacking (γ_{us}) energies and ductility parameter (D^{GB}) for the $\Sigma5(0\,1\,2)$ GB, for different concentrations Θ of S impurities. σ_t and σ_s are the corresponding tensile and shear strengths for the GB without or with S impurities.

Bulk Ni				$\Sigma5(0\,1\,2)$ GB			
Θ	0.0	0.33	1.0	Θ	0.0	0.25	1.0
γ_s (J m^{-2})	1.91	1.40	0.93	$\tilde{W}_s$ (J m^{-2})	3.56	3.06	2.24
γ_{us} (J m^{-2})	0.29	0.17	0.10	γ_{us} (J m^{-2})	0.30	0.63	1.24
$D = \gamma_s/\gamma_{us}$	6.6	8.2	9.3	$D^{GB} = \tilde{W}_s/\gamma_{us}$	11.86	4.86	1.80
				σ_t (GPa)	20.91	20.11	17.74
				σ_s (GPa)	6.41	7.84	15.04

of impurities leads to a change in the supercell volume, as described earlier. The formation energy of the GB, obtained by comparing the energies of the supercell with the GB and a supercell which has exactly the same geometry and number of Ni atoms but no GB, is $\Delta E^{GB} = 1.21\,\mathrm{J\,m^{-2}}$, which compares well with the results reported earlier for the same GB ($1.19\,\mathrm{J\,m^{-2}}$ [11]). The calculated energy difference includes both the energy change due to supercell volume relaxation and the structural changes introduced by the GB.

To determine the work of separation W_s, a cut is introduced at the GB between layers GB0 and GB1. Here the situation is more complicated than for the decohesion of the perfect Ni crystal discussed earlier. We consider two cases: in the first, denoted as W_s, all the atoms on the decohesion planes are held fixed; in the second, denoted as $\tilde{W}_s$, we allow relaxations on the planes on either side of the cut by fixing only one reference Ni atom in each cut plane. We discuss first the result of the case with fixed atoms, which are shown in figure 4(*b*). The fit using UBER allows us to extract the decohesion energy for $d \to \infty$. Table 2 summarizes the results. In the absence of impurities the decohesion energy of the GB is smaller than that of bulk (1 1 1) Ni by only 7%. This is reasonable since the exposed surfaces upon decohesion of the GB are the $(0\,\bar{2}\,1)$ crystal surfaces, which have higher surface energy than the (1 1 1) surface, but the reference structure in this case includes the GB, which itself is a higher energy structure than the ideal bulk crystal. When S impurities are added, W_s is lowered by 7% for $\Theta = 0.25$ (one S atom in the unit cell of the GB0 plane), and by 31% for $\Theta = 1.0$ (four S atoms in the unit cell of the GB0 plane). This is consistent with calculations for the cleavage energy reported by Sanyal *et al* [13]. The reduction in W_s is much smaller than the corresponding reduction of the decohesion energy in the ideal Ni crystal upon the incorporation of S impurities. When surface relaxation is included, the resulting work of separation $\tilde{W}_s$ is generally lower. In the absence of S impurities the difference between W_s and $\tilde{W}_s$ is negligible. With S impurities, the effect of relaxation is stronger, and the values of $\tilde{W}_s$ are lower than that of the pure GB by 14% and 37% for $\Theta = 0.25$ and 1.0, respectively. The relaxation of atoms on the two planes on either side of the cut is significant, especially that of the impurities: the relaxed S atoms move outward away from the exposed surface by 0.41 Å with respect to the three Ni atoms that are allowed to relax, and by 0.18 Å with respect to the fixed reference Ni atom.

3.3. Generalized-stacking-fault energy for bulk Ni

For the calculations of the generalized-stacking-fault energy, care has to be taken how the atoms are relaxed on the slip planes, as the supercell vector $\boldsymbol{a}_3$ is changed by $\boldsymbol{s}$ (see figure 3). We simulate the behavior of the bulk away from the slip plane by keeping the central plane of the supercell fixed. We allow relaxations along $\boldsymbol{a}_3$ but keep the positions of all slip plane atoms fixed along $\boldsymbol{a}_1$ and $\boldsymbol{a}_2$, while the remaining atoms are allowed to relax freely. These

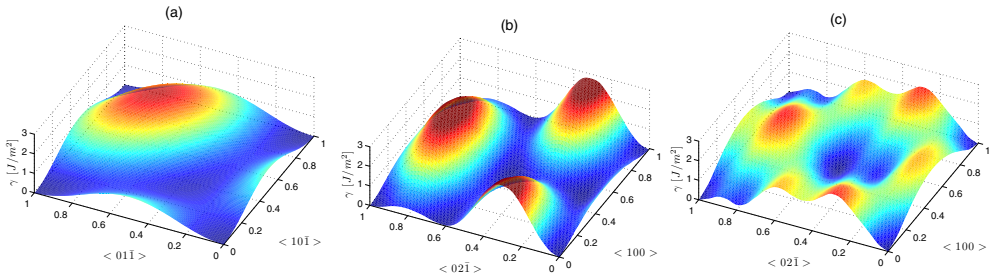

Figure 6. (*a*) Generalized-stacking-fault energy for slip on the (1 1 1) plane of bulk Ni (see the text for details). The lowest energy path between equivalent points on the slip plane lies in part along the diagonal direction in the plot; a displacement along this direction results in a partial dislocation with Burgers vector $\boldsymbol{b} = \frac{1}{6}\langle 1\,1\,\bar{2}\rangle$. (*b*) Generalized-stacking-fault energy for $\Sigma 5(0\,1\,2)$ GB in pure Ni and (*c*) in Ni with four interstitial S atoms on the GB plane (GB0), corresponding to $\Theta = 1.0$.

restrictions are crucial to ensure a meaningful representation of slip displacements that result in run-on configurations where atoms in the slip plane are directly on top of one another [27]. The resulting γ-surface for slip on the (1 1 1) plane is shown in figure 6(*a*). The (1 1 1) plane contains the minimal path between two equivalent slip points. The total slip between two such points results in a dislocation with Burgers vector $\boldsymbol{b}$ along the $\langle 1\,0\,\bar{1}\rangle$ direction, which can split into two partial dislocations with Burgers vectors $\boldsymbol{b}_1 = \frac{1}{6}\langle 1\,1\,\bar{2}\rangle$ and $\boldsymbol{b}_2 = \frac{1}{6}\langle 2\bar{1}\bar{1}\rangle$. Along these directions, the minimal energy barrier $\gamma_{\rm us}$ occurs at a relative displacement of $0.6\sqrt{6}a$ Å (see figure 6(*a*)); the slip energy along $\langle 1\,1\,\bar{2}\rangle$ is shown in figure 7(*a*). The intrinsic stacking fault energy obtained from this calculation is $\gamma_{\rm sf} = 0.143\,{\rm J\,m^{-2}}$, in good agreement with experimental results ($0.125\,{\rm J\,m^{-2}}$ [44]).

We performed convergence tests with respect to the size of the supercell in the $\boldsymbol{a}_3$ direction by increasing the size to 4 units along the $\boldsymbol{a}_3$ direction, which gave a difference of less than 1% to the results mentioned above. To confirm that the substitutional S atoms did not distort the supercell significantly we performed relaxations along $\langle 1\,1\,1\rangle$ in the case of added impurities. This resulted in a change in $\boldsymbol{a}_3$ of less than 1% for both $\Theta = 0.33$ and 1.0. Table 2 shows the values of the unstable stacking energy, $\gamma_{\rm us}$, for the case $\Theta = 0.0$, 0.33 and 1.0 on the slip plane: the presence of S produces a decrease in $\gamma_{\rm us}$ by 41% and 66% for $\Theta = 0.33$ and 1.0, respectively. This indicates that a slip becomes more favorable with increasing impurity concentration. In the context of Griffith cleavage, the decohesion energy results presented in section 3.1 suggested that the material should become more brittle since the energy barrier for creation of new surfaces decreases considerably as impurities are added. This is outweighed by the changes in the unstable stacking energy. The ductility parameter D increases by 24% and 41% for $\Theta = 0.33$ and 1.0, that is, with added S impurities bulk Ni actually should become more ductile. This is not seen in experiments when S impurities are added to Ni. These results already suggest that Ni embrittlement cannot be due to S incorporation in the bulk, but that instead other processes are dominant.

3.4. Generalized-stacking-fault energy at a GB

To model the resistance of a Ni GB against shear, we calculate its generalized-stacking-fault energy. We use the same structure as in section 3.2, but now displace all atoms of one of the two half-crystals, defined by a cut between GB0 and GB1, by a slip vector $\boldsymbol{s}$ (figure 5). As in the case of the generalized-stacking-fault energy calculations for bulk Ni, we relax the atoms of the slip plane in the $\boldsymbol{a}_3$ direction only and keep them fixed along $\boldsymbol{a}_1$ and $\boldsymbol{a}_2$; this allows us

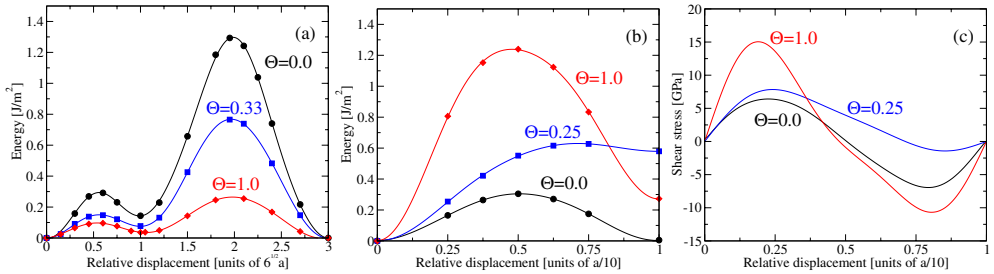

Figure 7. (*a*) The generalized-stacking-fault energy along the $\langle 1\,1\,\bar{2}\rangle$ path for slip on the (1 1 1) plane of bulk Ni, without ($\Theta = 0.0$) and with ($\Theta = 0.33$ and 1.0) S impurities. The relative displacement is in units of $\sqrt{6}a$, where a is the bulk lattice constant. The unstable stacking energy, γ_{us}, occurs at a relative displacement of $0.6\sqrt{6}a$. (*b*) The generalized-stacking-fault energy for the $\Sigma 5(0\,1\,2)$ GB, without ($\Theta = 0.0$) and with ($\Theta = 0.25$ and 1.0) S impurities. The relative displacement is in units of $\frac{a}{10}$ along $\langle 5\,2\,\bar{1}\rangle$ for $\Theta = 0.0$ and 0.25 and in units of $\frac{a}{10}$ along $\langle 5\,6\,\bar{3}\rangle$ for $\Theta = 1.0$. (*c*) The corresponding shear stress for the GB.

to define the slip vector $\boldsymbol{s}$ properly. Note that such a slip displacement defines two interfaces under our periodic boundary conditions: the first at GB0 and the second at GB10. Accordingly S impurities were added to both these planes in a symmetrical fashion. We again simulate a bulk layer by holding the center-most two planes between the two GBs fixed.

The γ-surface of the GB without S impurities is shown in figure 6(*b*). The three maxima in the energy surface correspond to run-on configurations of the Ni atoms in the GB0 and GB1 planes (compare with figure 5). A displacement by a slip vector $\boldsymbol{s} = \frac{a}{10}\langle 5\,2\,\bar{1}\rangle$ leads to a configuration that is geometrically equivalent to the initial GB structure. The maximum energy of the minimal energy path (see figure 7(*b*)) between these two geometrically equivalent points, corresponds to the unstable stacking energy $\gamma_{us} = 0.30\,\mathrm{J\,m^{-2}}$, which is almost the same as for the case of pure bulk Ni.

When impurities are added to the interstitial sites, the symmetry of the GB plane is altered and the possible slip vectors leading to minima in the γ-surface change. We have performed separate γ-surface calculations for structures with one ($\Theta = 0.25$) and four ($\Theta = 1.0$) interstitial S atoms on the GB plane, and determined the minimal energy path between equivalent points. For $\Theta = 0.25$, the minimal energy path follows the slip vector $\boldsymbol{s} = \frac{a}{10}\langle 5\,2\,\bar{1}\rangle$; this is the same as for $\Theta = 0.0$. When all interstitial sites on the GB plane are filled with S impurities ($\Theta = 1.0$), the direction to the nearest local minimum changes such that the minimal energy path now occurs along $\boldsymbol{s} = \frac{a}{10}\langle 5\,6\,\bar{3}\rangle$ (figure 6(*c*)). Due to the change of geometry of the GB plane when impurities are added, the slip vectors are now associated with partial GB dislocations. The respective minimal paths are plotted for $\Theta = 0.0$, 0.25 and 1.0 in figure 7(*b*). In contrast to the results for the bulk crystal, the value of γ_{us} increases with impurity inclusion (table 2). We can see from these results that GBS is suppressed with S impurity inclusion at the GB. Since GBS is a dominant process of plastic deformation in nc metals, this strongly suggests that such materials would behave less ductile when S segregates to the Ni GBs. The almost two- and four-fold increase in γ_{us} for $\Theta = 0.25$ and 1.0 results in a decrease of 59% and 85%, respectively, for the value of the ratio D^{GB} between the work of separation W_s and the unstable stacking energy γ_{us} (see table 2). This means that our results for the changes in W_s in combination with our findings for the shear behavior indicate that for a given individual GB interface we expect the mechanical behavior to change from a more ductile response involving GBS to a more brittle response involving cleavage along the GB.

In order to take into account changes in the minimal energy path with S inclusion, we calculate a ductility parameter $\tilde{D}^{GB}$ that includes geometry changes based on equation (1) by

Table 3. The values of the ductility parameter $\tilde{D}^{\mathrm{GB}}$ when the geometry change between $\Theta = 0.0$ ($\tilde{D}^{\mathrm{GB}}_0$) and 1.0 ($\tilde{D}^{\mathrm{GB}}_1$) is considered. The angle between the two possible Burgers vectors is $\Delta\phi = 29.21^\circ$. θ is the dihedral angle between the slip and decohesion plane.

Planes	$\theta(^\circ)$	$\tilde{D}^{\mathrm{GB}}_0$	$\tilde{D}^{\mathrm{GB}}_1$	$\tilde{D}^{\mathrm{GB}}_0/\tilde{D}^{\mathrm{GB}}_1$
$[(0\,1\,\bar{2}), (0\,1\,2)]$	53.1	0.658	0.330	2.0
$[(1\,2\,0), (0\,1\,2)]$	66.4	2.846	0.532	5.4
$[(2\,1\,0), (0\,1\,2)]$	78.5	0.658	0.424	1.6
$[(0\,\bar{2}\,1), (0\,1\,2)]$	90.0	0.642	0.322	2.0

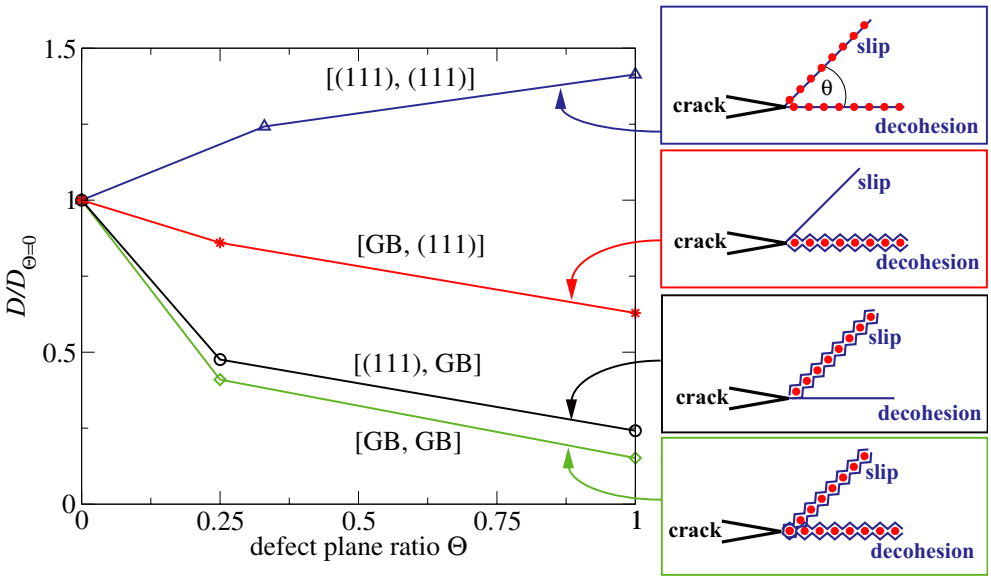

Figure 8. Normalized ductility parameter $D/D_{\Theta=0}$ for bulk Ni and Ni with a $\Sigma 5(0\,1\,2)$ GB. The four data sets shown are values of D for the relevant combinations of decohesion and slip planes, with labels [decohesion plane, slip plane] and their respective schematics to the right. The lines are guides for the eye.

considering the possible intersections of $\{0\,1\,2\}$ planes for the two different Burgers vectors [1]. This is presented in table 3. We find that for physically realistic configurations the behavior of $\tilde{D}^{\mathrm{GB}}$ remains unaffected and the trends are the same as for the more simplified ductility parameter D^{GB}, that is, S inclusion significantly decreases the value of D^{GB}.

It is possible that the GB may provide a relaxation mechanism in combination with the (1 1 1) planes. We plot in figure 8 the normalized ductility parameter D of such physically reasonable configurations. In this comparison, we have left out the possible combinations that have S impurities on the (1 1 1) planes together with GB slip or decohesion, since we have already seen in section 3 and table 1 that the thermodynamically most stable positions of the S impurity atoms are at the GB, which are energetically preferred by 1.3 to 1.6 eV, depending on S coverage, over bulk planes. We first consider that the GB could serve as a decohesion plane in combination with a clean (1 1 1) plane as the slip plane. Such a geometry would be of importance for coarse-grained systems but also for materials with heterogeneous grains. Due to the decrease in W_{s} of the GB with S inclusion, the ductility parameter of such a geometry also decreases. We see that therefore this mechanism also changes to more brittle behavior

[1] We assume here that the Poisson ratio is unchanged and takes the value $\nu = 0.276$ [44].

resulting in preferential intergranular fracture. The GB could also serve as a slip plane with decohesion on the (1 1 1) planes. Although this process would likely result in blunting of any emerging (1 1 1) crack in the intrinsically ductile bulk Ni, it is possible that such blunting is not a dominant effect in nc and ufc materials. This process of transgranular failure will therefore still be considered. We again see a decrease in D^{GB}, implying preferential brittle behavior, since ductile behavior in the form of GBS becomes energetically less favorable. Overall this comparison shows that S impurity segregation at the GB defects results in a decrease in the ductility parameter for all combinations involving the GB.

We have shown that for a system where GB slip and GB decohesion are considered as competing processes, S impurities segregated to the GB plane result in an overall more brittle response. The question that still remains is if our results support an increase of intergranular fracture, that is, if a crack can more easily propagate along the grains. A simple model, similar in spirit to that in [10], illustrates a possible intergranular fracture mechanism. We first calculate the shear and tensile strengths, that is, the maximum of the derivatives of the relevant energy curves of figures 4(*b*) and 7(*b*) with respect to displacement. This is shown in figures 4(*c*) and 7(*c*) and summarized in table 2. We see a small decrease in the tensile strength σ_{t} as S impurities are added to the GB. In contrast, the shear strength σ_{s} increases significantly. Although decohesion of the grains is preferred for S inclusion, a crack within this model can only propagate efficiently if GBS supports this. This is illustrated by the simple schematic of figure 1. If we assume that the force perpendicular to the cracked GB is equal to the critical value of the tensile strength, we find that for all possible $\Sigma 5(0\,1\,2)$ GB geometries the parallel forces required for sliding are larger than the critical shear strength. This implies decohesion, followed by sliding, leading to easy crack propagation. In contrast, when we add impurities the critical shear strength increases, and for $\Theta = 1.0$, two out of five possible geometries of our GB are now not supporting crack propagation anymore; intergranular crack propagation, at least when it is accommodated by GBS, is suppressed. Although our results for GBS suggest that this form of plastic deformation is suppressed with impurity inclusion at the GB, indicative of a more brittle behavior, this model predicts that the expected type of fracture behavior is not intergranular fracture. Several important points have to be made regarding these results. First, in our simple crack propagation model intergranular fracture accommodated by GBS is possible for the pure GBs. This does not imply intergranular fracture for pure nc Ni; instead we are limited to conclusions based on our $\Sigma 5(0\,1\,2)$ GB which is a special GB and any sample in an experiment would be made up of a variety of GBs intersecting at various angles. Treating GB properties from first-principles calculations is notoriously difficult due to the unknown structure at the GB and the large unit cells required. Thus, performing calculations over many possible GBs is not feasible. As in most similar studies, we have considered here a single GB structure and explored the implications of having impurities in it, with the expectation that this gives useful insight into the behavior of such systems. We assume that other GBs that share structural features with the one we studied, such as adequate space to accommodate the impurity atoms at low-energy positions, will exhibit similar behavior. We investigated only changes in the behavior of such special GBs as we add S impurities. For nc grains intergranular fracture behavior has been predicted by classical MD simulations without any impurity inclusion [15]. Second, we found that a fracture mode accommodated by GBS is suppressed. This does not preclude intergranular fracture in general, as it applies only GBS related mechanisms. Cracking along the grain will still occur once the applied forces for the perpendicular components of the GBs exceed the continuously decreasing critical tensile strength. We can therefore anticipate a behavior where initially the suppression of GBS increases brittle behavior, making both intergranular and transgranular fracture possible. For increasing S impurity concentrations, a decreasing value of W_{s} would eventually lead to pure intergranular fracture. In the context

of the competition between trans- and intergranular fracture, it is important to note that GB decohesion for $\Theta = 1.0$ gives a value of W_s which is almost half that of the decohesion energy for the (1 1 1) planes. This clearly makes GB decohesion and hence intergranular fracture an energetically preferred pathway.

The last issue we consider is the effect of S impurities on the crystalline order around the GB, which could be important in inducing fracture. This effect was first proposed by Heuer *et al* [9] and computationally treated by Chen *et al* [10]. They see that an amorphized GB results in a dramatic decrease in the shear strength as impurities are added, favoring immediate intergranular crack propagation as the GB is weakened both for cleavage and shear. Our results support the argument that this is indeed necessary to facilitate easy intergranular fracture accommodated by GBS for the Ni and S system. A more detailed analysis of a system of very high S impurity concentration that leads to amorphization of the GB region is beyond the scope of the present approach.

4. Conclusion

We have performed a first-principles DFT study of the mechanical behavior of fcc Ni in the presence of S impurities. The differences between bulk fcc Ni and fcc Ni with a $\Sigma5(0\,1\,2)$ GB defect as S impurities are added were investigated. Low-energy interstitial positions for the S impurity atoms at the GB are the stable sites, versus the substitutional defect sites in the bulk fcc crystal. This already highlights the importance of GBs in chemical embrittlement and is consistent with the experimentally observed S segregation to GBs [1–9].

We employ Rice's theory to investigate changes in the ratio of the surface and the unstable stacking energy (the ductility parameter D) to quantify changes in the ductility. This approach is adapted to our system with a $\Sigma5(0\,1\,2)$ GB by considering the competition between GB decohesion and shear in the form of GBS. GB decohesion, indicative of brittle behavior, is quantified through the work of separation (W_s), whilst GBS, a mechanism of plastic deformation in nc metals, is quantified through γ_{us}, analogous to previous work on GBs in crystalline solids [11–13]. By considering the energy of dislocation nucleation in the bulk and of GBS for our GB, in comparison with the decohesion energy and the work of separation, respectively, we are able to put this problem on a more complete and quantitative footing in the context of the competition between processes of cleavage and plastic deformation. Our calculations for the bulk defect-free structure indicate that an increase in ductility occurs as impurities are added. In contrast, we find that the resistance to shear, quantified by γ_{us}, increases for the GB structure. This limits plastic deformation and indicates a transition to brittle behavior, as this form of plastic deformation mechanism is removed. The effect of embrittlement persists when geometric factors are fully accounted for according to Rice's theory and when different combinations of slip and cleavage systems are considered. Although our results for the $\Sigma5(0\,1\,2)$ GB show that GBS is suppressed with S impurity segregation, intergranular cracking facilitated by GBS in our simple geometric model does not become more preferred. We do not see the significant decrease of shear strength observed in MD calculations of amorphized GBs [10]; amorphization is important to enable easy intergranular crack propagation that is accommodated by GBS. Our results address the problem of a crystalline GB since analyzing an amorphous GB in the context of Rice's theory is not feasible. We show that even before any possible amorphization of the GB is considered, there is clear evidence for a significant decrease in ductility but not in the form of immediate intergranular fracture accommodated by GBS. This does not preclude intergranular fracture for large enough tensile forces, since the tensile strength decreases with the inclusion of S impurities. Any failure mode that relies on GBS is suppressed for the GB system.

Acknowledgments

This work was funded in part by a graduate fellowship from the Harvard Graduate Consortium on Energy and Environment and support from the Department of Energy, SciDac Grant ER-25788. The authors would like to thank the SEAS Academic Computing Group and the FAS Research Computing Group for computational resources. The authors wish to acknowledge useful discussions with Gang Lu, James Rice, Frans Spaepen and Priya Vashishta.

References

[1] Loier C and Boos J-Y 1981 *Metall. Trans.* A **12** 1223
[2] Floreen S and Westbrook J H 1969 *Acta Metall.* **17** 1175
[3] Johnson W C, Doherty J E, Kear B H and Giamei A F 1974 *Scr. Metall.* **8** 971
[4] Doherty J E, Giamei A F and Kear B H 1974 *Can Metall. Q.* **13** 229
[5] Lozinskiy M G, Volkogon G M and Pertsovskiy N Z 1967 *Russ. Met.* **5** 65
[6] Kobayashi S, Tsurekawa S, Watanabe T and Palumbo G 2010 *Scr. Mater.* **62** 294
[7] Lassila D H and Birnbaum H K 1987 *Acta Metall* **35** 1815
[8] Bruemmer S M, Jones R H, Thomas M T and Baer D R 1983 *Metall. Trans.* A **14** 223
[9] Heuer J K, Okamotoa P R, Lam N Q and Stubbins J F 2000 *Appl. Phys. Lett.* **76** 3403
[10] Chen H-P, Kalia R K, Kaxiras E, Lu G, Nakano A, Nomura K, van Duin A C T, Vashishta P and Yuan Z 2010 *Phys. Rev. Lett.* **104** 155502
[11] Yamaguchi M, Shiga M and Kaburaki H 2005 *Science* **307** 393
[12] Kart H H, Uludogan M and Cagin T 2009 *Comput. Mater. Sci.* **44** 1236
[13] Sanyal S, Waghmare U V, Subramanian P R and Gigliotti M F X 2008 *Appl. Phys. Lett.* **93** 223113
[14] Van Swygenhoven H and Derlet P M 2001 *Phys. Rev.* B **64** 224105
[15] Farkas D, Van Swygenhoven H and Derlet P M 2002 *Phys. Rev.* B **66** 060101(R)
[16] Bachurin D V and Gumbsch P 2010 *Acta Mater.* **58** 5491
[17] Kumar K S, Van Swygenhoven H and Suresh S 2003 *Acta Mater.* **51** 5743
[18] Schiøtz J, Di Tolla F D and Jacobsen K W 1998 *Nature* **391** 561
[19] Schiøtz J, Vegge T, Di Tolla F D and Jacobsen K W 1999 *Phys. Rev.* B **60** 11971
[20] Armstrong R W 1966 *Mater. Sci. Eng.* **1** 251
[21] Kelly A, Tyson W R and Cottrell A H 1967 *Phil. Mag.* **15** 567
[22] Rice J R and Thomson R 1974 *Phil. Mag.* **29** 73
[23] Rice J R 1992 *J. Mech. Phys. Solids* **40** 239
[24] Peierls R E 1940 *Proc. Phys. Soc.* **52** 34
[25] Sun Y M, Beltz G E and Rice J R 1993 *Mater. Sci. Eng.* A **170** 67
[26] Kaxiras E and Duesbery M S 1993 *Phys. Rev. Lett.* **70** 3752
[27] Juan Y M and Kaxiras E 1996 *Phil. Mag.* A **74** 1367
[28] Sun Y M and Kaxiras E 1997 *Phil. Mag.* A **75** 1117
[29] Bulatov V V and Kaxiras E 1997 *Phys. Rev. Lett.* **78** 4221
[30] Waghmare U V, Kaxiras E, Bulatov V V and Duesbery M S 1998 *Modelling Simul. Mater. Sci. Eng.* **6** 493
[31] Waghmare U V, Kaxiras E and Duesbery M S 2000 *Phys. Status Solidi* b **217** 545
[32] Thomson R 1995 *Phys. Rev.* B **52** 14245
[33] Vitek V 1968 *Phil. Mag.* **18** 773
[34] Kresse G and Furthmüller J 1996 *Phys. Rev.* B **54** 11169
[35] Perdew J P, Burke K and Ernzerhof M 1996 *Phys. Rev. Lett.* **77** 3865
[36] Kresse G and Joubert D 1999 *Phys. Rev.* B **59** 1758
[37] Methfessel M and Paxton A T 1989 *Phys. Rev.* B **40** 3616
[38] Monkhorst H J and Pack J D 1976 *Phys. Rev.* B **13** 5188
[39] Mehl M J and Papaconstantopoulos D A 1996 *Phys. Rev.* B **54** 4519
[40] Lu G, Orlikowksi D, Park I, Politano O and Kaxiras E 2002 *Phys. Rev.* B **65** 064102
[41] Evans R C 1964 *An Introduction to Crystal Chemistry* (Cambridge: Cambridge University Press)
[42] Udagawa Y, Yamaguchi M, Abe H, Sekimura N and Fuketa T 2010 *Acta Mater.* **58** 3927
[43] Rose J H, Smith J R, Guinea F and Ferante J 1984 *Phys. Rev.* B **29** 2963
[44] Hirth J P 1982 *Theory of Dislocations* 2nd edn (New York: Wiley)